Visible light enhanced photothermal CO$_2$ hydrogenation over Pt/Al$_2$O$_3$ catalyst

ZHAO Ziyan [a,b], Dmitry E. DORONKIN [c,d,*], YE Yinghao [b], Jan-Dierk GRUNWALDT [c,d,*] HUANG Zeai [a,b], ZHOU Ying [a,b,*]

[a] State Key Laboratory of Oil and Gas Reservoir Geology and Exploitation, School of Materials Science and Engineering, Southwest Petroleum University, Chengdu 610500, Sichuan, China

[b] The Center of New Energy Materials and Technology, School of Materials Science and Engineering, Southwest Petroleum University, Chengdu 610500, China

[c] Institute for Chemical Technology and Polymer Chemistry (ITCP), Karlsruhe Institute of Technology, Karlsruhe (KIT), 76131 Karlsruhe, Germany

[d] Institute of Catalysis Research and Technology (IKFT), Karlsruhe Institute of Technology (KIT), 76344 Eggenstein-Leopoldshafen, Germany

Abstract: Light illumination has been widely applied to promote activity and selectivity of traditional thermal catalysts. Nevertheless, the role of light irradiation during catalytic reactions is not well understood. In this work, Pt/Al$_2$O$_3$ prepared by wet impregnation was used for photothermal CO$_2$ hydrogenation, and it showed a photothermal effect. Hence, operando diffuse reflectance infrared Fourier-transform spectroscopy (DRIFTS) and density functional theory (DFT) calculations were conducted on Pt/Al$_2$O$_3$ to reveal insight into the reaction mechanism. The results indicated that CO desorption from Pt sites including step sites (Pt$_{step}$) or/and terrace site (Pt$_{terrace}$) is an important step during CO$_2$ hydrogenation to free the active Pt sites. Notably, visible light illumination and temperature affected CO desorption in different ways. The calculated adsorption energy of CO on Pt$_{step}$ and Pt$_{terrace}$ sites was -1.24 and -1.43 eV, respectively. Hence, CO is stronger bound to Pt$_{step}$ sites. During heating process in the dark, CO preferentially desorbs from Pt$_{terrace}$ site. However, the additional light irradiation facilitates transfer of CO from Pt$_{step}$ to Pt$_{terrace}$ sites and its subsequent desorption from the Pt$_{terrace}$ sites, thus promoting CO$_2$ hydrogenation.

Key words: CO$_2$ hydrogenation; photothermal catalysis; Pt/Al$_2$O$_3$, operando DRIFTS, DFT

1. Introduction

With the developments of industry and economy, great attention is being paid to environment remediation [1-4]. Emissions of carbon dioxide as a primary greenhouse gas result in global temperature increase and climate changes. Among the numerous CO_2 utilization strategies, CO_2 hydrogenation attracted extensive attention because it provides not only an important strategy for environmental improvement, but also a promising technology to produce renewable hydrocarbon fuels such as $HCOOH$, CH_3OH and CH_4 [5-10]. However, high temperature is generally required for CO_2 hydrogenation due to the thermodynamic stability of CO_2 [11-13].

Photothermal catalysis, a combination of photoexcitation with thermal energy to trigger chemical reactions, allows significant improvements in activity and selectivity of catalytic reactions as well as stability of the catalysts [5, 14-16]. Therefore, light irradiation has been utilized to promote diverse thermal catalytic reactions such as CO oxidation [17], propylene oxidation [18], Fischer-Tropsch Synthesis [19], reverse water gas shift (RWGS) reaction [20] and CO_2 hydrogenation [21]. Light irradiation can significantly improve the catalytic performance during these reactions. For instance, in our previous work, we found that the light irradiation promoted CO oxidation through O_2 excitation [22]. Wang et al. reported that photo-induced back donation of electrons from Co to CO facilitated CO activation and dissociation [19]. In addition, visible light irradiation increased RWGS activity of Au nanoparticles by 1300% while decreasing activation energy from 47 to 35 $kJ*mol^{-1}$ [20]. For CO_2 hydrogenation, light induced electron transfer from Rh to anti-bonding orbitals of a reaction intermediate resulted in efficient CH_4 generation [15]. CO desorption was regarded as the rate-limiting step during CO_2 hydrogenation [23]. However, the effects of light and temperature on this step are still not deeply understood.

In this work, CO_2 hydrogenation was conducted over Pt/Al_2O_3 catalyst. Operando diffuse reflectance infrared Fourier transform spectroscopy (DRIFTS) was applied to investigate CO desorption on Pt sites during photothermal CO_2 hydrogenation process. The reaction pathway was discussed to understand the mechanism of photothermal catalysis.

2. Experimental

2.1. Catalyst synthesis

Pt/Al_2O_3 catalysts were prepared using wet impregnation method with aqueous H_2PtCl_6 as described in our previous work [24]. γ-Al_2O_3 (10 nm) was bought from Aladdin Co., Ltd. 500 mg γ-Al_2O_3 was dispersed in a mixture of 5 mL H_2PtCl_6 (2 mg/mL) solution and 30 mL water to achieve 2 wt.% Pt loading on γ-Al_2O_3. Then the suspension was stirred for 6 h at 27 °C. The product was centrifuged and dried at 65 °C for 24 h. Pt/TiO_2 was prepared in the same way using hydrothermally synthesized anatase TiO_2 support as used by our previous work [22] and described in the Supporting Information.

2.2. Characterization

X-ray diffraction (XRD) patterns were recorded on a PANalytical X'pert diffractometer using Cu Kα

radiation operating at 40 mA and 40 kV. Transmission electron microscopy (TEM) was carried out on a FEI Tecnai G2 20 microscope operating at 200 kV. UV-vis spectra were recorded on a Shimadzu 2600 UV−vis spectrophotometer. Raman spectra were obtained on a Horiba LabRAM HR Evolution with a 532 nm laser.

2.3 CO_2 hydrogenation evaluation and operando DRIFTS

Sieved powder catalysts (approx. 50 mg, sieve fraction: 100-200 μm) were used for the tests. The catalysts were pretreated in 5% H_2/He (100 mL/min) at 200 °C for 6 h. The temperature of the catalyst bed was calibrated by an IR camera. During activity evaluations, 1000 ppm CO_2 and 6000 ppm H_2 in He were dosed into the reactor (Harrick Praying Mantis™ high temperature reaction chamber with a flat cover and a quartz window, Scheme 1, left) at 110 mL/min. Schott KL 2500 LCD light source with an intensity of 710 mW/cm^2 was used as light source. CO and CO_2 concentrations were detected by a Hartmann & Braun Uras 10E detector. The photo enhancement was calculated as following: Photo enhancement = (Rate$_{photothermal}$-Rate$_{thermal}$)/Rate$_{thermal}$. OmniStar GSD-320 quadrupole mass spectrometer (Pfeiffer Vacuum) was used to detect CO (m/z=28), CO_2 (m/z=44), CH_3OH (m/z=31), HCOOH (m/z= 46) and CH_4 (m/z=16).

For operando DRIFTS the gas composition was kept the same as for catalytic tests. The spectra were measured on a VERTEX 70 FTIR spectrometer (Bruker) equipped with a mercury cadmium telluride (MCT) detector. Harrick in situ cell with a dome cover with two KBr and a glass window was used as the reactor (Scheme 1, right). The catalyst was pretreated in 5% H_2/He with the flow rate of 100 mL/min at 200 °C for 6 h. The spectra of the pre-reduced catalysts at 30 °C in pure He gas were used as background spectra. The reaction conditions were stabilized for 30 min without light at room temperature, and then DRIFTS spectra were collected (without light) at 30, 80, 120, 160 and 200 °C. After the spectra obtained at each temperature point, the catalyst was irradiated during 10 min. Then it was first flushed with He and the spectra were recorded after the He flushing. At each temperature, the catalyst was flushed with He gas for 10 and 20 min, and then additional spectra were collected. IR scanning range was 4000 ~ 700 cm^{-1} with 4 cm^{-1} resolution and averaging over 100 scans.
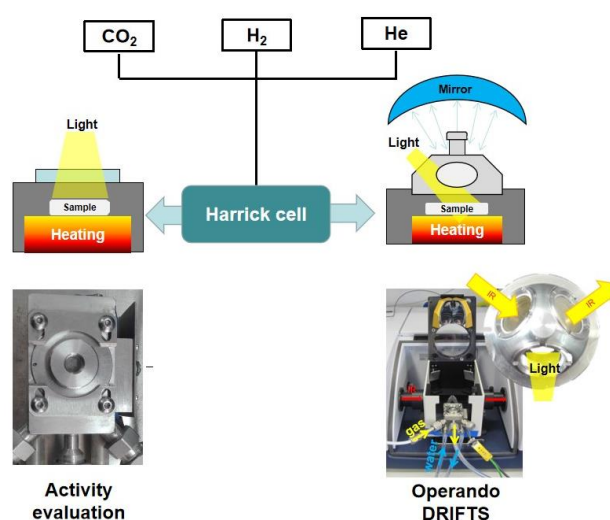
Scheme 1. Scheme of the setup for CO_2 hydrogenation activity evaluation and operando DRIFTS investigation.

2.4 Thermodynamic calculation

Equilibrium concentrations of species obtained during CO_2 hydrogenation were calculated by HSC chemistry 7 [25]. The ratio of CO_2/H_2 was 1/6, CHOOH, CH_3OH, CO, H_2O and CH_4 were originally considered as products. Including CH_4 in the calculation led to the conclusion that is the preferred product under thermodynamic control with an equilibrium concentration near 100% among all carbon-containing species at all studied temperatures [26]. Since only a small amount of CH_4 was detected experimentally, it's production is limited by kinetics. Therefore, it was excluded from further thermodynamic analysis.

2.5 Computational details

Density functional theory (DFT) calculations were performed using $DMol^3$ procedure based on Materials Studio software. The electron exchange and correlation were approximated by generalized gradient approximation (GGA) with the Perdew-Burke-Ernzerhof (PBE) functional. Dispersion correction by TS (DFT-D) was used to describe the van der Waals interaction. The valence electron configurations were $2s^2 2p^2$ for C, $2s^2 2p^4$ for O and $5d^9 6s^1$ for Pt, respectively. As for the Monkhorst-Pack grid k-point in the Brillouin-zone, a $5 \times 5 \times 1$ k-point was used for geometry optimizations. For convergence threshold, the total energy of the system, maxforce, and displacement tolerances were set to be 1×10^{-5} Ha, 0.02 Ha/Å, and 0.05 Å, respectively. A space of 15 Å vacuum was set between slabs in order to avoid interaction.

The adsorption energy (E_{ad}) of adsorbates was calculated as follows:

$$E_{ad} = E_{CO+surface} - E_{surface} - E_{CO} \qquad (1)$$

where $E_{CO+surface}$ is the total energy of Pt surface with CO, $E_{surface}$ is the total energy of the clean surface, and E_{CO} is the total energy of CO in the gas phase. The CO molecule was optimized in a three-dimensional (3D) box of a=b=c=15 Å.

3. Results and discussion

3.1. Photothermal effects

CO_2 conversion rate and CO production rate during CO_2 hydrogenation over Pt/Al_2O_3 at different temperatures are depicted in Fig. 1. As shown in Fig. 1a, during thermal catalysis CO_2 conversion rate increased from 0 to 10 $\mu mol*g^{-1}min^{-1}$ when temperature changed from 80 to 120 °C, and up to about 225 $\mu mol*g^{-1}min^{-1}$ at 400 °C. CO was not detected until the temperature increased to 200 °C (Fig. 1b). Additional light irradiation significantly promoted both CO_2 conversion and CO production rates. For example, CO_2 conversion rate with light at 120 °C was about 50 $\mu mol*g^{-1}min^{-1}$ while it was only 10 $\mu mol*g^{-1}min^{-1}$ in the dark. CO production rate was ca. 0 $\mu mol*g^{-1}min^{-1}$ at 120 °C in the dark and about 15 $\mu mol*g^{-1}min^{-1}$ under light irradiation (Fig. 1b). The rates measured at other temperatures were also significantly promoted by light. Moreover, light irradiation decreased the temperature required for CO generation on Pt/Al_2O_3. CO production rate at 120 °C under light was close to the thermal activated CO

production rate at 250 °C, and a similar trend was also observed for CO_2 conversion rates. Photo enhancement was used to evaluate the effect of light on thermal driven reaction, the enhancement reached the maximum value at 80 °C at about 9 times compared to the corresponding purely thermal driven CO_2 conversion rate. As the temperature rose, thermal-induced rate further increased while the photo-induced enhancement decreased, which may be due to mass-transfer limitations [23].

On the other side, temperature increase due to light irradiation should also be taken into consideration. In our previous work, although light intensity was 972 mW/cm^2, light irradiation increased the surface temperature by no more than 60 °C [22]. In this work, at lower light intensity 710 mW/cm^2, both CO_2 and CO rates over Pt/Al_2O_3 at 80 °C under light irradiation were much higher than the rates at 160 °C in the dark. Therefore, Pt/Al_2O_3 exhibited typical synergistic effect of photoexcitation and thermal energy. Since the used $\gamma\text{-}Al_2O_3$ support material is a typical insulator and could not take part in the electron transfer process under light irradiation, Pt should provid active sites for CO_2 hydrogenation.

To investigate the support effect, the alumina support was replaced by a typical photocatalyst, TiO_2. As shown in Fig. S1a, CO_2 conversion rate over Pt/TiO_2 increased from 10 to 250 $\mu mol*g^{-1}min^{-1}$ when temperature increased from 80 to 400 °C. These rates were also significantly promoted by light irradiation. For example, the CO_2 conversion rate was 50 $\mu mol*g^{-1}min^{-1}$ at 80 °C with light on while it was only about 10 $\mu mol*g^{-1}min^{-1}$ in the dark. Moreover, the light induced CO_2 conversion rate, 50 $\mu mol*g^{-1}min^{-1}$, was identical to the rate measured at 250 °C in the dark. The CO_2 conversion and CO production rates over Pt/TiO_2 were similar to those of Pt/Al_2O_3. The slightly higher activity of Pt/TiO_2 may be due to strong interaction between the Pt and TiO_2 support resulting in higher dispersion of Pt and inhibition of sintering [24]. Obviously, both catalysts exhibited very small differences in catalytic activity. Besides, Al_2O_3, as a support with high surface area facilitates high dispersion of Pt even without strong-metal support interaction. Moreover, with the wide band gap it can not be excited by light, which allows to decouple photoexcitation of Pt species and the photocatalytic effect of titania. Thus, the following investigations of the mechanism of CO_2 hydrogenation on Pt sites were conducted on Pt/Al_2O_3.
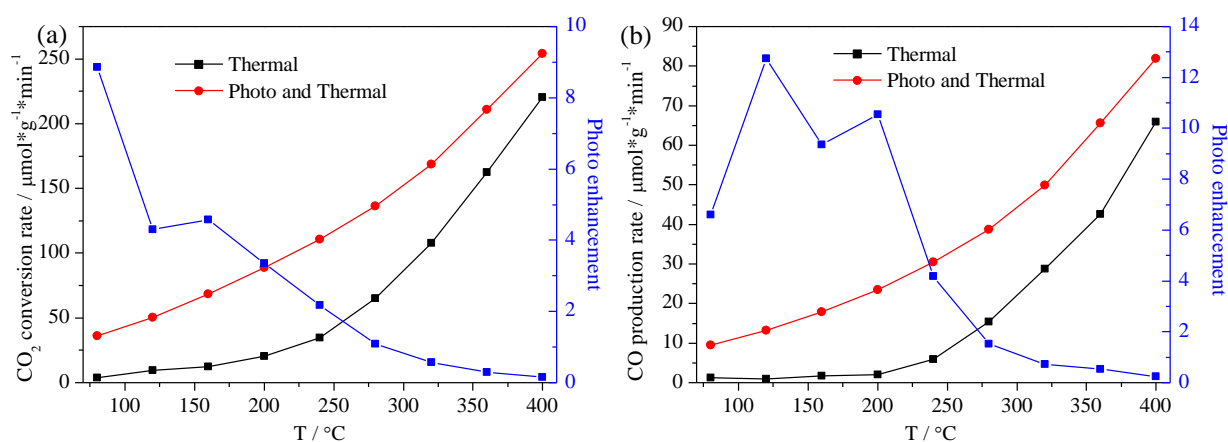
Fig. 1. a) CO_2 and b) CO conversion rates of photothermal CO_2 hydrogenation on Pt/Al_2O_3.

3.2. Products of CO_2 hydrogenation

According to Fig. 2a, the CO_2 conversion rate of Pt/Al_2O_3 increased from 32 to 75 $\mu mol*g^{-1}min^{-1}$, and then decreased to 30 $\mu mol*g^{-1}min^{-1}$ while the temperature increased from 80 to 400 °C. Meanwhile, CO production rate increased from 8 to 25 $\mu mol*g^{-1}min^{-1}$ and then decreased to 15 $\mu mol*g^{-1}min^{-1}$. Obviously, the consumed CO_2 was not totally converted into CO. To evaluate the composition of CO_2 hydrogenation products the outlet gas was analyzed by mass spectrometry (Fig. 2b) and the ion currents of some reactants and products are summarized in Fig. S2. Once CO_2 and H_2 feed was switched on higher H_2O, CH_4, and HCOOH background was detected. Further heating resulted in the corresponding increase in CH_4 and H_2O signals while CO_2 and HCOOH signals decreased. These results indicate that CO_2 and H_2 gradually converted into CH_4 and H_2O, and HCOOH may have been consumed as the reaction intermediate.
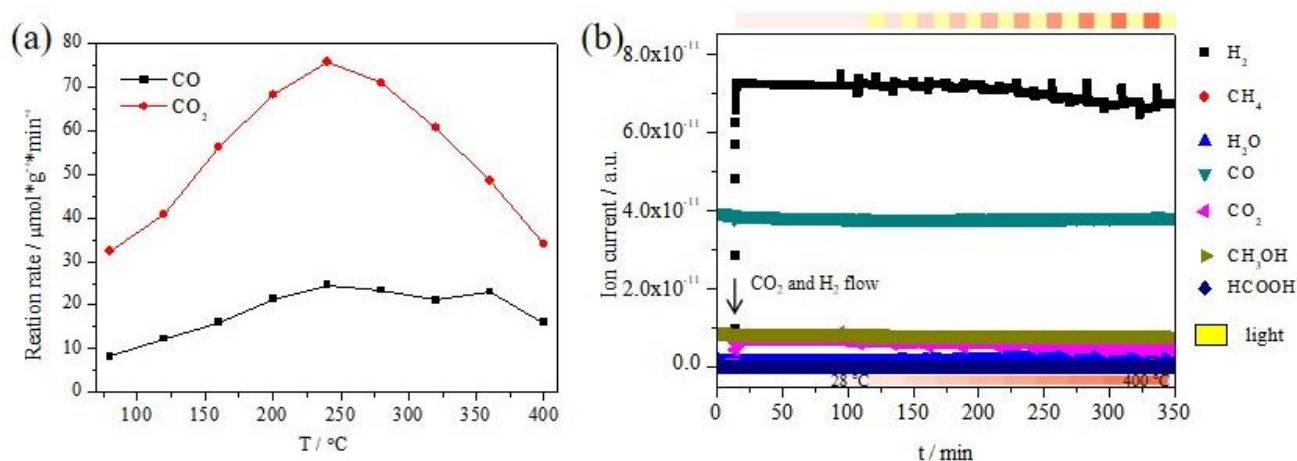
Fig. 2. a) CO_2 conversion and CO production rates of Pt/Al_2O_3 induced by light irradiation (after subtracting the corresponding thermally induced rates); b) Ion currents of products of CO_2 hydrogenation over Pt/Al_2O_3 measured at different temperatures in the dark and under light irradiation.

Thermodynamic equilibrium calculation for the used gas feed (molar ratio $CO_2:H_2=1:6$) is shown in Fig. 3. Three ranges can be observed during heating process. Below 120 °C CH_3OH is the thermodynamically preferred product of CO_2 hydrogenation (note that CH_4, if included in the calculation, would be the most thermodynamically stable through the whole studied temperature range). Although HCOOH is thermodynamically less stable than the other products, it was experimentally detected and its concentration was decreasing with increasing temperature. In the range of 120 to 180 °C, CO_2 is the most thermodynamically stable component, hence its reduction is not favored in this temperature range, as was also confirmed experimentally giving the low conversion rates. When temperature was above 180 °C, CO_2 conversion rate gradually increased, and CO production (reverse water gas shift reaction) is favored, consistent with the experimental CO_2 and CO rates changes shown in Fig. 3a. As shown in Fig. S2, the ion currents of reactants and products obtained from experimental results exhibited similar trends to the calculation. Thus, the thermodynamic calculation agrees well with the experimental results, and these results indicated that CO_2 hydrogenation is not limited by kinetics (unlike the CH_4 pathway).
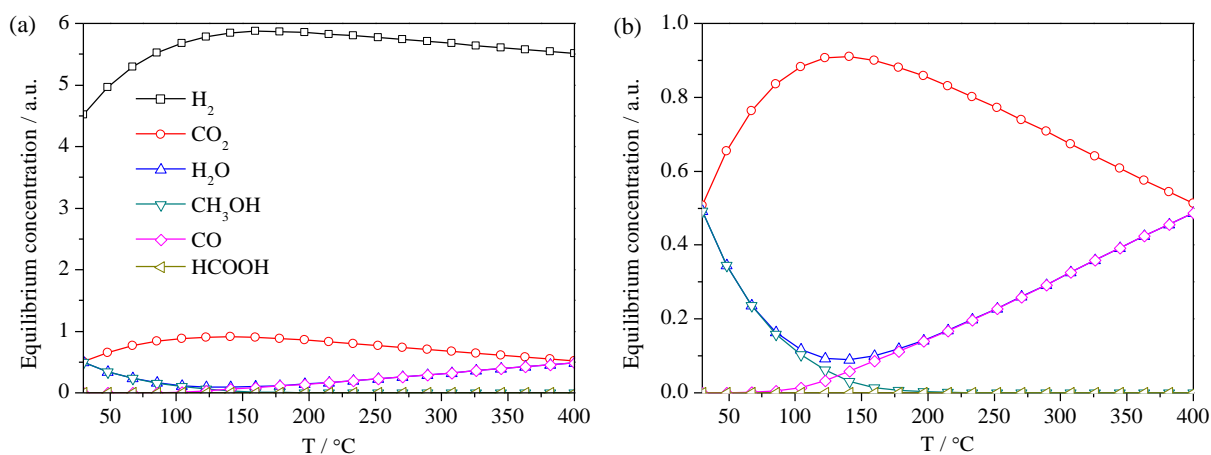
Fig. 3. Relative thermodynamic stability of species in the system including CO_2 (initial concentration 1), H_2 (initial concentration 6), and CO, HCOOH, CH_3OH, H_2O (initial concentrations of the four latter species were 0). a) Temperature dependent equilibrium concentrations of all considered reactants and products except CH_4; b) The enlarged trends of CO_2, CO, CH_3OH and H_2O from a).

3.3. Structure, morphology and optical properties

Pt was not detected in the XRD patterns (Fig. 4a), and all diffraction peaks were attributed to γ-Al_2O_3 (PDF#16-0394). TEM images (Fig. 4b) showed Pt nanoparticles with a diameter of 0.9 ± 0.2 nm deposited on Al_2O_3, and the crystalline interplanar spacing of 0.226 and 0.195 nm were indexed to {111} and {200} facets of Pt while the 0.289 nm was attributed to {117} facet of γ-Al_2O_3. As reflected by UV-vis spectra (Fig. S3), Pt deposition promoted the light adsorption ability of Al_2O_3 in the range of 200 ~ 600 nm [27]. For Pt/TiO_2, also the strong interaction at the Pt/TiO_2 interface was evidenced [24]. Raman spectra showed a signal located at 145 cm^{-1} assigned to the $E_g(1)$ peak of anatase (spectrum given in the supporting information, Figure S4). After Pt deposition, this peak shifted to 151 cm^{-1} which indicated the generation of Pt-$O_{vancancy}$-Ti^{3+} at the interface between Pt and TiO_2 [28]. Hong et al. [29] reported that Pt-$O_{vancancy}$-Ti^{3+} worked as an adsorption site for the reaction intermediates, such as CO generated from HCOOH decomposition. This increased residence time of surface intermediates resulting in the promoted activity. It might be also the reason that Pt/TiO_2 (Fig. S1) exhibited higher activity than Pt/Al_2O_3 (Fig. 1).
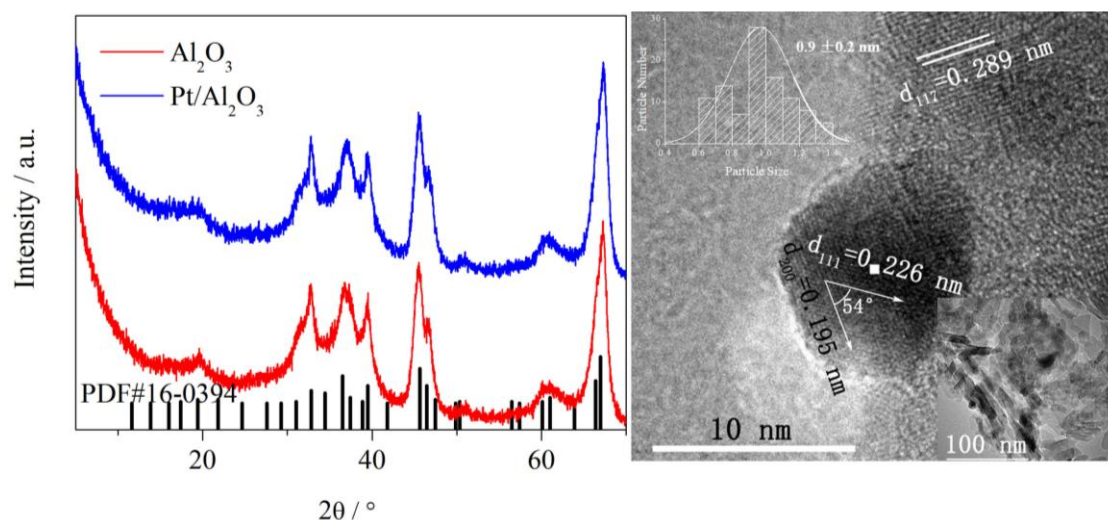
Fig. 4. a) XRD patterns and b) a representative HRTEM image of Pt/Al_2O_3 (with a histogram showing size distribution of Pt nanoparticles).

3.4. Operando DRIFTS

Operando DRIFTS spectra measured during photothermal catalytic CO_2 hydrogenation are shown in Fig. 5 and the assignments of IR peaks are summarized in Table 1. The maximum temperature was 200 °C to obtain reasonable signal-to-noise ratio.

Table 1   Assignments of peaks in IR spectra during CO_2 hydrogenation

Wavenumber/ cm^{-1}	Assignment	Reference
2326 ~ 2362	CO_2	[30]
2058 ~ 2046	CO $Pt_{terrace}$	[31,32]
2038 ~ 2007	CO Pt_{step}	[31] [32]
2007	CO on Pt_{step}	[32][33]
1760	Bridged CO	[31]
1625	-OH	[32,34]

As shown in Fig. 5a, after exposure of Pt/Al_2O_3 to CO_2 and H_2 at 30 °C peaks emerged at 2326 ~ 2362 and 1625 cm^{-1} which were attributed to CO_2 and -OH on Pt [30,32,34]. These signals became weaker and peaks at 2007 and 1760 cm^{-1} corresponding to carbonyl and CO evolved as temperature increased from 30 to 200 °C [31-33]. During temperature increase to 120 °C, CO production was not observed (Fig. S2d) in agreement with thermodynamics (Fig. 3b) while HCOOH decreased (Fig. S2e) and the intensity of carbonyl band at 2007 cm^{-1} (Fig. 5a) did not increase. Increase in the catalyst temperature resulted in higher intensity of the carbonyl band at 2007 cm^{-1}. Considering the gradual decrease of HCOOH concentration in the effluent (Fig. S2e) and increase CO concentration (in Fig. 1, Fig. 2 and Fig. 3), the higher band intensity was attributed to the CO produced on Pt_{step} site [31,32].

Under light illumination below 80 °C the intensity of 1624 cm^{-1} band (surface -OH) decreased (Fig. 5b), and the signals in the range of 2326 ~ 2362 cm^{-1} (CO_2) slightly increased while the peaks at 2007 cm^{-1} and 1760 cm^{-1} (CO) obviously rose [30-33]. Besides, CO_2 and HCOOH ion currents decreased as shown in Fig. S2a and Fig. S2e. These changes indicate that CO_2 preferred to adsorb on Pt and then form small amount of CO under light irradiation. At temperatures above 120 °C, CO generation was promoted by temperature and CO molecules gradually accumulated on Pt_{step} sites without light. With light turned on at the respective temperatures, CO signals were significantly increased indicating the promoted CO generation (Fig. 5b), in accordance with increased concentration of CO in the gas phase (Fig. 1b and Fig. S2d). Noteworthy, the CO signal at 2007 cm^{-1} was blue shift once the light was turned on indicating that

interaction of CO molecules with Pt_{step} sites weakened.
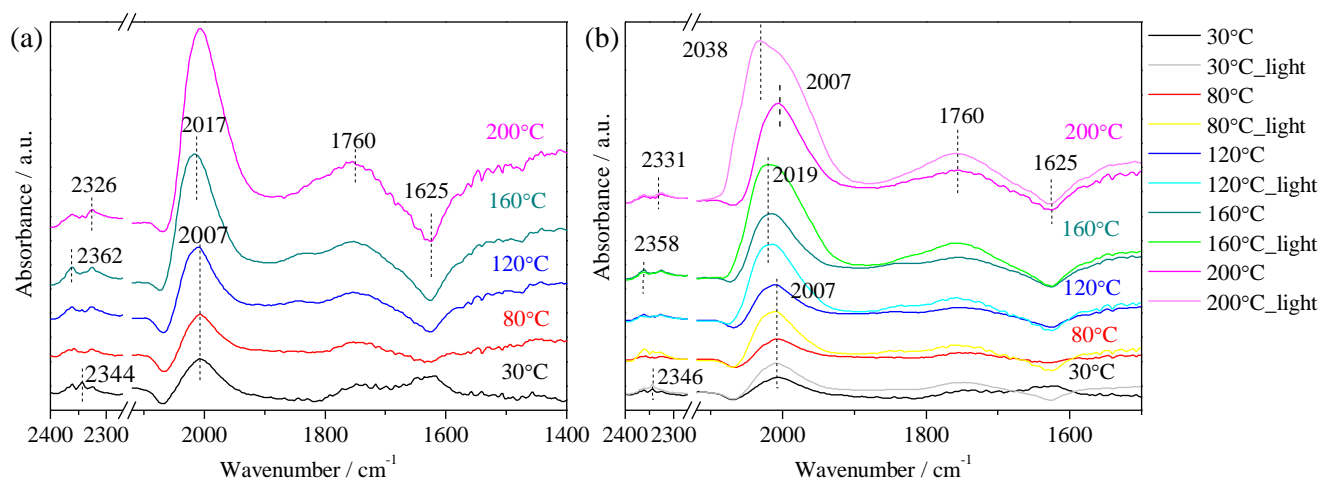
Fig. 5. Operando DRIFTS spectra of Pt/Al_2O_3 during a) thermal and b) photothermal CO_2 hydrogenation

To further investigate the interaction between CO and Pt, helium was used to flush the catalyst surface to observe the intermediate species adsorbed during photothermal CO_2 hydrogenation (Fig. 6). CO on Pt_{step} sites (2038 ~ 2007 cm^{-1} [31,32]) was not visible after He flushing. But CO on $Pt_{terrace}$ sites was detected in the range of 2058 ~ 2046 cm^{-1} different to the thermal catalysis shown in Fig. 5a [31,32]. That indicates that light and temperature have different effects on CO adsorption. CO adsorbs on Pt_{step} sites much stronger compared to $Pt_{terrace}$ sites, desorption from which was found to occur at approx. 350-450 K [35]. As shown in Fig. 1b, small amount of CO evolved at temperature below 200 °C in the dark, hence the generated CO probably desorbed from $Pt_{terrace}$ sites and the corresponding signals could not be observed in the IR spectra (Fig. 5a). On the other hand, CO was adsorbed stronger on undercoordinated Pt_{step} sites resulting in clearly visible IR bands. Even when the temperature reached 200 °C the produced CO was still accumulated on Pt_{step} sites as reported in previous research [36]. Thus, the observed CO on $Pt_{terrace}$ in Fig. 6 was not originating during thermal catalysis but during light irradiation.
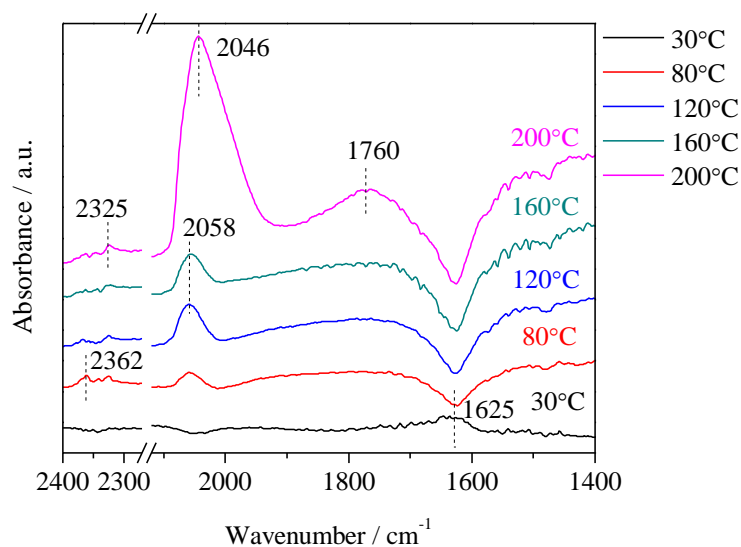
Fig. 6. Operando DRIFTS spectra of Pt/Al$_2$O$_3$ with 20 min flushing with He gas after turning off light

3.5. Effects of light and temperature on CO$_2$ desorption

According to the mechanism of CO$_2$ hydrogenation [37], CO desorption is regarded as an important step with activation energy of CO desorption from Pt and Pd much higher than from other metals [23]. At low temperatures the active sites on metal surface are usually covered by CO which poisons or blocks the sites [38,39]. Hence, CO desorption from the active sites is required to free sites catalyzing CO$_2$ hydrogenation. The operando DRIFTS results indicated that light and temperature affected CO desorption in different ways. Formed CO preferred to desorb from Pt$_{terrace}$ sites during heating while its distribution seem to be altered under additional light irradiation.

Compared to the terrace sites, metal step sites are more coordinatively more unsaturated which is beneficial for CO adsorption [40,41]. To further reveal the interaction between CO and Pt, energies of CO adsorption on Pt$_{terrace}$ and Pt$_{step}$ sites were calculated by DFT. Adsorption geometries and the corresponding energies are shown in Fig. 7. Pt-C distances for CO adsorbed on Pt$_{terrace}$ and Pt$_{step}$ sites were 2.01 and 1.98 Å and the adsorption energies were -1.24 and -1.43 eV, respectively, which were similar to the reported -1.39 and -1.42 eV in the previous work [42]. This indicates that CO adsorbs stronger on Pt$_{step}$ sites than Pt$_{terrace}$ sites, consistent with IR results [43,44]. As shown in Fig. 5b and Fig. 6, light irradiation weakens the interaction between CO and Pt$_{step}$ sites. But, even after helium flushing CO on Pt$_{terrace}$ site with weaker bonding was still detected during the photothermal process in the range of 30 ~ 200 °C while the CO on Pt$_{step}$ site was not visible. This indicates that CO desorbed from Pt$_{step}$ sites while the produced CO accumulated on Pt$_{terrace}$. Additionally, Lawrenz et al. [45] reported that laser light could induce the spillover of CO from Pt$_{step}$ to Pt$_{terrace}$ sites. Thus, with the light irradiation, produced CO first transfers from Pt$_{step}$ sites to Pt$_{terrace}$ sites and then desorbs from Pt$_{terrace}$ sites.
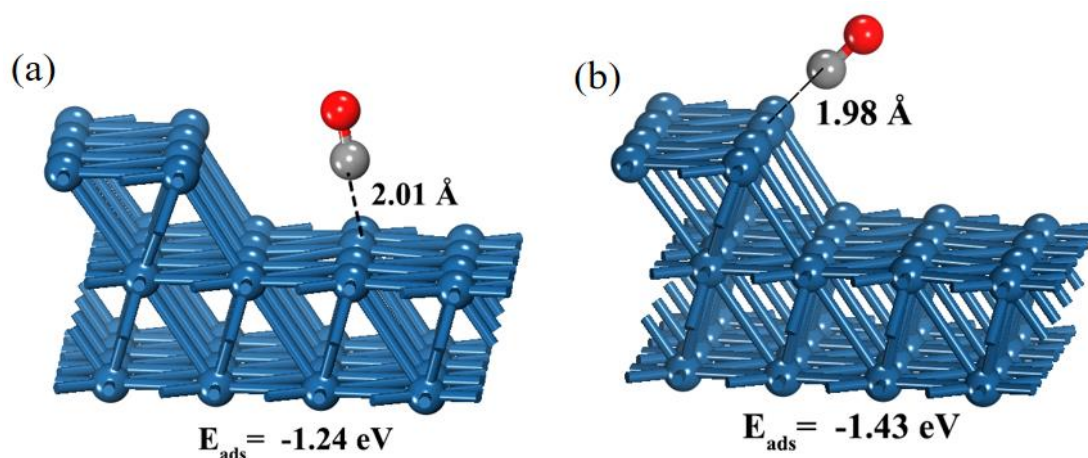
Fig. 7. Adsorption energies and Pt-C distances for CO adsorbed on a) Pt$_{terrace}$ and b) Pt$_{step}$

Based on the results mentioned above, main reactions occurring during CO$_2$ hydrogenation were summarized in eq. (2-5), and the mechanism of light and temperature activation of CO desorption from Pt

during CO_2 hydrogenation is summarized in Fig. 8. CO_2 and H_2 are spontaneously converted to HCOOH due to the low activation energy [46]. Subsequently, HCOOH is decomposed to *CO adsorbed on $Pt_{terrace}$ (E_{ads} = -1.24 eV) and Pt_{step} (E_{ads} = -1.43 eV) sites. CO desorption is regarded as a crucial step during CO_2 hydrogenation to free the active low-coordinated Pt step sites. Considering the weaker interaction between CO and $Pt_{terrace}$ sites, generated CO preferred to desorb from $Pt_{terrace}$ site in thermally activated CO_2 hydrogenation process [36]. On the contrary, additional light irradiation induced CO desorption from Pt_{step} sites (with possible spillover to $Pt_{terrace}$ sites) as evidenced by operando DRIFTS. As a result, the interaction between CO and Pt site became weaker and further thermally activated CO desorption from $Pt_{terrace}$ site was facilitated. Hence we suggest that this, in turn, promotes CO_2 hydrogenation [45,47], which should be further substantiated in future studies.

$$CO_2 + H_2 \rightarrow HCOOH \qquad\qquad (2)$$

$$HCOOH \rightarrow *CO + *H_2O \qquad\qquad (3)$$

$$*CO + *H_2O + H \rightarrow *H_2COH \text{ or } *H_3CO \qquad\qquad (4)$$

$$*H_2COH \text{ or } *H_3CO \xrightarrow{H+H_2O} CH_4 \text{ and } CH_3OH \qquad\qquad (5)$$
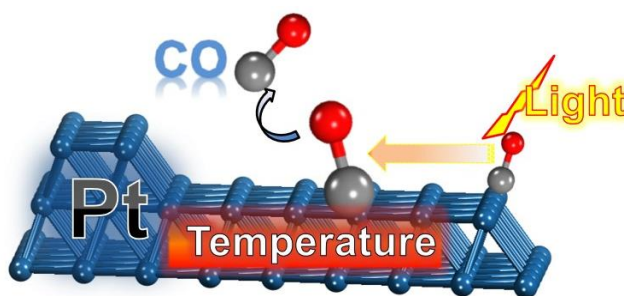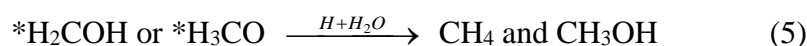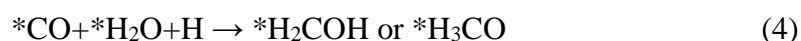
Fig. 8. Light and temperature effect on the CO desorption during CO_2 hydrogenation on different Pt sites

4. Conclusions

Pt/Al_2O_3 was synthesized through impregnation method. It exhibited photothermal catalytic activity in CO_2 hydrogenation with Pt providing active sites. Operando DRIFTS and theoretical calculations indicated that light and temperature facilitated CO desorption from Pt in different ways. CO preferentially desorbed from $Pt_{terrace}$ sites during thermal activation. With the additional light irradiation, CO on Pt_{step} site transferred to $Pt_{terrace}$ site, and then its thermal desorption from $Pt_{terrace}$ site was facilitated. As a result, CO desorption activated by both heating process and additional light irradiation resulted in the promotion of CO_2 hydrogenation. This work provides further understanding of the effect of light and temperature on CO desorption during CO_2 hydrogenation, and may help in designing more efficient photothermal catalytic processes in future.

References

[1] S. Stojadinović, R. Vasilić, N. Radić, N. Tadić, P. Stefanov, B. Grbić, *Appl. Surf. Sci.,* **2016**, 377, 37-43.

[2] X. Wang, C. Liu, X. Li, F. Li, Y. Li, J. Zhao, R. Liu, *Appl. Surf. Sci.,* **2017**, 394, 340-350.

[3] H. Wang, H. Qi, X. Wei, X. Liu, W. Jiang, *Chin. J. Catal.,* **2016**, 37, 2025-2033.

[4] H. Wang, W. He, X. Dong, H. Wang, F. Dong, *Sci. Bull.,* **2018**, 63, 117-125.

[5] M. D. Porosoff, B. H. Yan, J. G. G. Chen, *Energ. Environ. Sci.*, **2016**, 9, 62-73.

[6] K. Li, B. S. Peng, T. Y. Peng, *ACS Catal.*, **2016**, 6, 7485-7527.

[7] Y. A. Daza, J. N. Kuhn, *RSC Adv.*, **2016**, 6, 49675-49691.

[8] X. Li, J. Yu, M. Jaroniec, X. Chen*, Chem. Rev.*, **2019**, 119, 3962-4179.

[9] W. Wang, D. Xu, B. Cheng J. Yu, C. Jiang, *J. Mater. Chem. A.,* **2017**, 5, 5020-5029.

[10] H. Zhao, J. Chen, G. Rao, W. Deng, Y. Li, *Appl. Surf. Sci.,* **2017**, 404, 49-56.

[11] W. Wang, S. P. Wang, X. B. Ma, J. L. Gong, *Chem Soc Rev.*, **2011**, 40, 3703-3727.

[12] W. H. Li, H. Z. Wang, X. Jiang, J. Zhu, Z. M. Liu, X. W. Guo, C. S. Song, *RSC Adv.*, **2018**, 8, 7651-7669.

[13] S. Saeidi, N. A. S. Amin, M. R. Rahimpour, *J. CO$_2$ Util.*, **2014**, 5, 66-81.

[14] J. Jia, H. Wang, Z. L. Lu, P. G. O'Brien, M. Ghoussoub, P. Duchesne, Z. Q. Zheng, P. C. Li, Q. Qiao, L. Wang, A. Gu, A. A. Jelle, Y. C. Dong, Q. Wang, K. K. Ghuman, T. Wood, C. X. Qian, Y. Shao, C. Y. Qiu, M. M. Ye, Y. M. Zhu, Z. H. Lu, P. Zhang, A. S. Helmy, C. V. Singh, N. P. Kherani, D. D. Perovic, G. A. Ozin, *Adv Sci.*, **2017**, 4, 1700252-1700264.

[15] X. Zhang, X. Q. Li, D. Zhang, N. Q. Su, W. T. Yang, H. O. Everitt, J. Liu, *Nat. Commun.*, **2017**, 8, 14542-14550.

[16] P. Chen, F. Dong, M. Ran, J. Li, *Chin. J. Catal.,* **2018**, 39, 619-629.

[17] B. T. Qiao, A. Q. Wang, X. F. Yang, L. F. Allard, Z. Jiang, Y. T. Cui, J. Y. Liu, J. Li, T. Zhang, *Nat. Chem.*, **2011**, 3, 634-641.

[18] A. Marimuthu, J. W. Zhang, S. Linic, *Science.*, **2013**, 339, 1590-1593.

[19] L. M. Wang, Y. C. Zhang, X. J. Gu, Y. L. Zhang, H. Q. Su, *Catal. Sci. Technol.*, **2018**, 8, 601-610.

[20] A. A Upadhye, I. Ro, X. Zeng, H. J. Kim, I. Tejedor, M. A. Anderson, J. A. Dumesic, G. W. Huber, *Catal. Sci. Technol.*, **2015**, 5, 2590-2601.

[21] W. B. Zhang, L. B. Wang, K. W. Wang, M. U. Khan, M. L. Wang, H. L. Li, J. Zeng, *Small.*, **2017**, 13, 1602583-1602587.

[22] Y. Zhou, D. E. Doronkun, Z. Y. Zhao, P. N. Plessow, J. Jelic, B. Detlefs, T. Pruessmann, F. Studt, J. D. Grunwaldt, *ACS Catal.*, **2018**, 8, 11398-11406.

[23] J. K. Nørskov, T. Bligaard, J Rossmeisl, C. H. Christensen, *Nat. Chem.*, **2009**, 1, 37-46.

[24] Y. Zhou, D. E. Doronkin, M. L. Chen, S. Q. Wei, J. D. Grunwaldt, *ACS Catal.*, **2016**, 6, 7799-7809.

[25] A. Roine, Outokumpu HSC Chemistry for Windows Version 7 Outokumpu, **2015.**

[26] J. L. White, M. F. Baruch, J. E. Pander, Y. Hu, I. C. Fortmeyer, J. E. Park, T. Zhang, K. Liao, J. Gu, Y. Yan, T. W. Shaw, E. Abelev, A. B. Bocarsly, *Chem. Rev.*, **2015**, 115, 12888-12935.

[27] S. Sarina, H. Y. Zhu, Q. Xiao, E. Jaatinen, J. F. Jia, Y. M. Huang, Z. F. Zheng, H. S. Wu, *Angew. Chem. Int. Edit.*, **2014**, 53, 2935-2940.

[28] Z. C. Lian, W. C. Wang, G. S. Li, F. H. Tian, K. S. Schanze, H. X. Li, *ACS Appl. Mater. Inter.*, **2017**, 9, 16959-16966.

[29] S. S. Kim, K. H. Park, S. C. Hong, *Fuel. Process. Technol.*, **2013**, 108, 47-54.

[30] W. Wasylenko, H. Frei, *Phys. Chem. Chem. Phys.*, **2007**, 9, 5497-5502.

[31] H. Yoshida, S. Narisawa, S. Fujita, L. Ruixia, M. Arai, *Phys. Chem. Chem. Phys.,* **2012**, 14, 4724-4733.

[32] M. J. S. Farias, G. A. Camara, J. M. Feliu, *J. Phys. Chem. C.*, **2015**, 119, 20272-20282.

[33] J. Scalbert, F. C. Meunier, C. Daniel, Y. Schuurman, *Phys. Chem. Chem. Phys.,* **2012**, 14, 2159-2163.

[34] T. Iwasita, F. Nart, *Prog. Surf. Sci.*, **1997**, 554, 271-340.

[35] H. R. Siddiqui, X. Guo, I. Chorkendorff, J. T. Yates, *Surf. Sci.*, **1987**, 191, L813-L818.

[36] S. S. Kim, H. H. Lee, S. C. Hong, *Appl. Catal. A.*, **2012**, 423-424, 100-107.

[37] M. D. Porosoff, B. H. Yan, J. G. G. Chen, *Energy Environ. Sci.*, **2016**, 9, 62-73.

[38] G. Ertl, *Angew. Chem. Int. Edit.*, **2008**, 47, 3524-3535.

[39] A. Boubnov, A. Gänzler, S. Conrad, M. Casapu, J. D. Grunwaldt, *Top. Catal.*, **2013**, 56, 333-338.

[40] H. C. Wu, Y. C. Chang, J. H. Wu, J. H. Lin, I. K. Lin, C. S. Chen, *Catal. Sci. Technol.*, **2015**, 5, 4154-4163.

[41] J. H. Kwak, L. Kovarik, J. Szanyi, *ACS Catal.*, **2013**, 3, 2449-2455.

[42] R. B. Sandberg, M. H. Hansen, J. K. Nørskov, F. Abild-Pedersen, M. Bajdich, *ACS Catal.*, **2018**, 8, 10555-10563.

[43] B. Shan, Y. J. Zhao, J. Hyun, N. Kapur, J. B. Nicholas, K. Cho, *J. Phys. Chem. C.*, **2009**, 113, 6088-6092.

[44] J. T. Niu, X. S. Du, J. Y. Ran, R. R. Wang, *Appl. Surf. Sci.*, **2016**, 376, 79-90.

[45] M. Lawrenz, K. Stépán, J. Güdde, U. Höfer, *Phys. Rev. B.*, **2009**, 80, 75429-75432.

[46] L. Dietz, S. Piccinin, M. Maestri, *J. Phys. Chem. C.*, **2015**, 119, 4959-4966.

[47] K. Golibrzuch, P. R. Shirhatti, J. Geweke, J. Werdecker, A. Kandratsenka, D. J. Auerbach, A. M. Wodtke, C. Bartels, *J. Am. Chem. Soc.*, **2015**, 137, 1465-1475.

可见光增强Pt/Al$_2$O$_3$催化剂光热CO$_2$氢化性能

赵梓俨 [a,b], Dmitry E. Doronkin [c], 叶英浩 [b], Jan-Dierk Grunwaldt [c,d,*] 黄泽皑[a,b], 周莹 [a,b,*],

[a]西南石油大学油气藏地质及开发工程国家重点实验室, 四川成都610500

[b]西南石油大学材料科学与工程学院新能源材料及技术研究中心，四川成都610500

[c]德国卡尔斯鲁厄理工学院化学技术与高分子化学研究所，德国卡尔斯鲁厄76131

[d] 德国卡尔斯鲁厄理工学院催化研究与技术研究所，德国卡尔斯鲁厄76344

摘要: 光照已被广泛应用于优化传统热催化剂的反应活性和选择性。然而，光激发在催化反应过程中作用尚未得到很好地理解。本文通过浸渍法制备 Pt/Al$_2$O$_3$，并应用于光热 CO$_2$ 氢化反应，Pt/Al$_2$O$_3$ 体现出了光热协同效应。结合原位漫反射红外光谱(DRIFTS)和理论计算(DFT)对 Pt/Al$_2$O$_3$ 的反应机理进行进一步研究。研究结果表明，CO 从 Pt 纳米颗粒的台阶位置(Pt$_{step}$)或/和平台位置(Pt$_{terrace}$)脱附是 CO$_2$ 氢化反应过程中的重要一步，有利于暴露出 Pt 反应活性位点。值得注意的是，光照和温度对 CO 脱附具有不同影响。计算结果证明，CO 吸附在 Pt$_{step}$ 和 Pt$_{terrace}$ 上时的吸附能分别为-1.24 和-1.43 eV。因

此，CO 与 Pt$_{step}$ 的相互作用力更强。在无光条件下的升温过程中，CO 更容易从 Pt$_{terrace}$ 位置发生脱附。但是当在对应温度下加入光照条件时，有利于 Pt$_{step}$ 上吸附的 CO 先转移到 Pt$_{terrace}$，然后从 Pt$_{terrace}$ 上发生脱附，从而有利于 CO$_2$ 氢化反应的进行。本研究有利于更加深入理解光热催化机理，研究结果可以作为进一步优化热催化反应的机制。

关键词： 二氧化碳氢化；光热催化；铂/三氧化二铝；原位红外光谱；第一性原理

*通讯联系人. 电话: (49)72160842120；传真: (49)72160844820；电子信箱: jan-dierk grunwaldt@kit.edu

*通讯联系人. 电话: (49)72160842120；传真: (49)72160844820；电子信箱: dmitry.doronkin@kit.edu

#通讯联系人. 电话: (028)83037411；传真: (028)83037406；电子信箱: yzhou@swpu.edu.cn

The manuscript title

Light and temperature effects on CO desorption during photothermal CO_2 hydrogenation over Pt/Al_2O_3

Ziyan Zhao, Dmitry E. Doronkin, Yinghao Ye, Ying Zhou*, Jan-Dierk Grunwaldt*

Affiliation: Southwest Petroleum University; Karlsruhe Institute of Technology
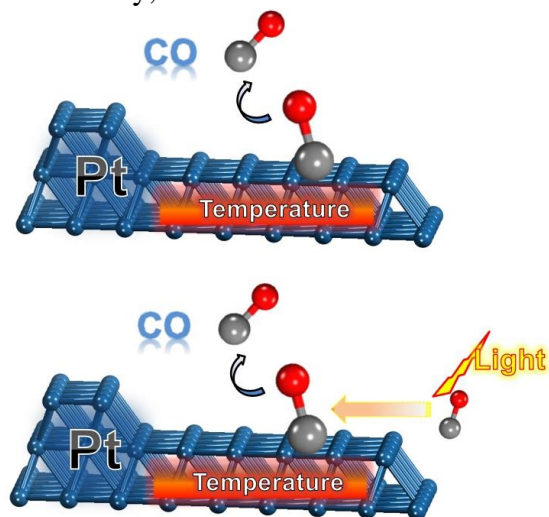
Light illumination and temperature affected CO coverage during CO_2 hydrogenation in different ways, offering a new pathway for improving thermal catalysis.